Marine Geology 343 (2013) 15–28

Contents lists available at ScienceDirect

Marine Geology

journal homepage: www.elsevier.com/locate/margeo

Quantifying overwash flux in barrier systems: An example from Martha's Vineyard, Massachusetts, USA

Emily A. Carruthers [1], D. Philip Lane [2], Rob L. Evans *, Jeffrey P. Donnelly, Andrew D. Ashton

Department of Geology and Geophysics, Woods Hole Oceanographic Institution, Woods Hole, MA 02543, United States

ARTICLE INFO

Article history:
Received 18 September 2012
Received in revised form 28 May 2013
Accepted 31 May 2013
Available online 14 June 2013

Communicated by J.T. Wells

Keywords:
overwash flux
barrier system
sea-level rise
storm impacts
coastal evolution

ABSTRACT

Coastal barriers are particularly susceptible to the effects of accelerated sea-level rise and intense storms. Over centennial scales, barriers are maintained via overtopping during storms, which causes deposition of washover fans on their landward sides. Understanding barrier evolution under modern conditions can help evaluate the likelihood of future barrier stability. This study examines three washover fans on the undeveloped south shore of Martha's Vineyard using a suite of vibracores, ground penetrating radar, high resolution dGPS, and LiDAR data. From these data, the volumes of the deposits were determined and range from 2.1 to 2.4×10^4 m^3. Two of these overwash events occurred during Hurricane Bob in 1991. The water levels produced by this storm have a calculated return interval of ~28 years, implying an onshore sediment flux of 2.4–3.4 m^3/m/yr. The third washover was deposited by a nor'easter in January 1997, which has a water level return interval of ~6 years, suggesting a flux of 8.5 m^3/m/yr. These onshore fluxes are smaller than the erosional flux of sediment resulting from shoreline retreat, suggesting that the barrier is not in long-term equilibrium, a result supported by the thinning of the barrier in recent years.

1. Introduction

Barriers form 10–13% of the world's coastlines (Cromwell, 1971; Stutz and Pilkey, 2011), with 76% of barriers occurring along rifted continental margins, like that of the US Atlantic Coast, which have wide depositional shelves, a wide flat coastal plain, and large supplies of available sediment (Inman and Nordstrom, 1971; Glaeser, 1978). Most barrier islands are located in areas that have undergone marine transgression, a rise in relative sea level causing a shift of the shoreline in the landward direction (Davis, 1985). In order for barriers to retreat and be sustained during conditions of sea-level rise, sediment must be transported from the nearshore and foreshore of the barrier to the backbarrier (Fisher and Simpson, 1979). Mechanisms for this landward sediment transport include transport through tidal inlets, including those of temporary inlets cut by storms, overwash of sand during storms, and aeolian transport (Boothroyd et al., 1985; Leatherman, 1985). The importance of overwash is amplified as sea-level rise accelerates because an increased rate of transgression typically leads to more frequent overwash events (Viles and Spencer, 1995). Different locations along the coast are influenced by unique combinations of sea-level rise rates, tidal range, storm tracks, wind and wave regimes, and sediment supply such that the dominant mechanism of barrier retreat is unique to each environment (Leatherman, 1985). On undeveloped coasts overwash typically dominates, causing barriers to "roll over" (Dillon, 1970; Dolan and Godfrey, 1973; Schwartz, 1975; Byrnes and Gingerich, 1987). Overwash is most frequent on the Atlantic and Gulf coasts of the US along sandy barriers. Here, it results from a combination of hurricanes and winter northeast storms (Donnelly et al., 2006).

Numerous studies have quantitatively explored barrier evolution. These models of barrier transgression are typically geometric modifications and extensions of the Bruun (1962) rule based upon the maintenance of an equilibrium shoreface shape. Mass conservation suggests that a wave-affected shoreline will recede as well as passively flood in response to sea-level rise; oversteepening of the shoreface causes sediment to migrate offshore. In the absence of overwash, the shoreline is expected to retreat according to the slope of the shoreface. Over longer timescales, and when overwash occurs, barrier coasts are expected to respond to sea-level rise in more complex ways. Equilibrium geometry concepts predict a more rapid shoreline retreat for transgressing barriers than for a shoreline without a barrier (Dean and Maurmeyer, 1983). Analytical approaches based on mass and shape conservation demonstrate that over transgressional timescales the morphology landward of the barrier controls the ultimate path of the shoreline, and the shoreface slope becomes unimportant (Wolinsky and Murray, 2009). This behavior can be seen in other numerical models of geometric barrier evolution due to sea-level rise over centennial and longer timescales (Cowell et al., 1995; Stolper et al., 2005; Moore et al., 2010). Morphodynamic modeling (Ashton and Ortiz, 2011) demonstrates that overwash and shoreface fluxes are intimately coupled, and that over hundreds to thousands of years timescales, overwash must dominate barrier response (and be sufficiently high) for barriers to remain

* Corresponding author. Tel.: +1 5082892673.
E-mail address: revans@whoi.edu (R.L. Evans).
[1] Now at: Sea Education Association, Woods Hole, United States.
[2] Deceased.

0025-3227/$ – see front matter © 2013 Elsevier B.V. All rights reserved.
http://dx.doi.org/10.1016/j.margeo.2013.05.013

intact during sea-level rise. Correspondingly, a barrier in equilibrium with sea-level rise has shoreface fluxes directed onshore to compensate for overwash fluxes.

Estimates of global sea-level rise by 2100 range from 75 cm to 190 cm over the time period of 1990 to 2100 (Vermeer and Rahmstorf, 2009) compared to the observed 26 ± 2 cm of sea-level rise at Woods Hole, MA over the last 100 years (NOAA, 2011c). This estimate may be as much as 20–30% higher in New England due to the complexities of the effect of the decreased gravitational pull of the large ice sheets, particularly the Antarctic, if they melt rapidly (Mitrovica et al., 2009). Evidence is also mounting for an increase in the frequency of intense storms in the North Atlantic (Emanuel et al., 2008). In light of this, it is important to understand the amount of sediment that is transferred to the backbarrier by overwash under present conditions in order to predict how this flux may change in the future. This study uses sediment cores and high-resolution geophysical surveys to estimate the volume of sediment contained in selected washover fans. These volumes are combined with estimates of return intervals of inundation levels to estimate the onshore sediment flux caused by major storms. The aim in doing so is to establish whether or not the studied section of barrier is in equilibrium with rising sea levels or whether it is likely to drown. In carrying out this study, we explain methodologies that can be exported to other settings.

1.1. Overwash processes and deposits

Overwash is the process by which storm surge, wave set-up, and wave run-up cause a flow of sediment-laden water to overtop a barrier, transporting sediment to the backbarrier. Washover refers to the deposit of sediment landward of the beach caused by overwash (Schwartz, 1975). There are two end-member causes of overwash: run-up overwash and inundation overwash (Donnelly et al., 2006). Run-up overwash occurs when wave run-up (the maximum vertical extent of wave up-rush on a beach) overtops a barrier. The resulting washovers are typically small and generally fan-shaped (Fig. 1) (the overwash regime of the Sallenger (2000) impact scale; Donnelly et al., 2006). When many small fans are deposited along a short stretch of barrier, the landward portions may join, forming a washover terrace (Fig. 1). Run-up overwash usually results from smaller storms than inundation overwash and usually happens in the hours surrounding high tide (Fisher and Stauble, 1977; Leatherman et al., 1977). Tidal inlets can also be formed by these same processes, but typically occur where backbarrier slopes are steep and backbarrier tidal flats are small or absent (Pierce, 1970). Inundation overwash occurs when water levels rise over the top of the barrier causing the resulting washovers to be large sheets extending 100s to 1000s of meters wide (Fig. 1) (the elevation regime of the Sallenger (2000) impact scale; Donnelly et al., 2006). Sheet overwash typically occurs when barriers are small and uniformly low (Orford et al., 2003) or when extreme storms cause unusually high surges (Fisher and Stauble, 1977). Overwash can result from a combination of run-up and inundation mechanisms and often exploits low areas such as relict washovers, dune blowouts, and anthropogenic paths (Fisher and Simpson, 1979). The low point, or throat (Fig. 1), constricts the overwash flow and funnels it into the backbarrier where the flow expands and slows causing sediment carried by the flow to be deposited into a fan shape. When this fan extends into a backbarrier lagoon or pond it is sometimes referred to as a washover delta (Leatherman, 1976).

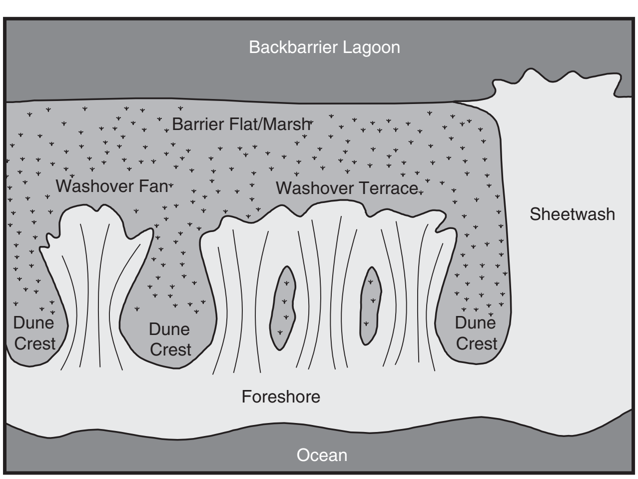

Fig. 1. Schematic of various types of washovers described in text. After Donnelly et al. (2006).

Overwash does not happen as a single episode of sediment overtopping the barrier, but as a succession of events potentially spanning the hours, or even days, of overtopping (Leatherman, 1976). These multiple events are recorded in washovers as laminations throughout the deposits (Schwartz, 1975; Leatherman, 1983), though these are not always seen in sediment cores (Leatherman et al., 1977; Boothroyd et al., 1985). The initial events of overwash can erode the throat and pre-overwash surface in the backbarrier, resulting in a reactivation surface (Pierce, 1970; Kochel and Dolan, 1986). This erosional surface can be observed in sediment cores if the washover extends into a backbarrier lagoon or pond as an abrupt contact between the washover sands and underlying mud (Donnelly et al., 2001a,b). This contact and the internal laminations of the washover can also be seen clearly using ground penetrating radar (GPR) (Buynevich et al., 2004; Baker et al., 2007).

The size of the washovers is determined by the path and strength of the storm, particularly surge and waves (Kochel and Dolan, 1986; Liu and Fearn, 2000). The size and shape of the deposit is also controlled by backbarrier morphology and vegetation (Donnelly et al., 2006). Leatherman (1976, 1979a) indicates that the volume of the washover is most dependent on storm surge height with the other factors holding less importance. Morton and Sallenger (2003) note that washover volumes are related to the type of washover, increasing from confined fans, to terraces, to sheet overwash deposits.

1.2. Previous studies of washover volumes

Previous research on washover volumes has largely been conducted on barriers on the mid-Atlantic Coast, specifically on or near Assateague Island, MD (see Table 1 for details). These studies have typically relied on a combination of sediment cores, aerial photos, and topographic profiles to estimate deposit volume. Some use only average washover thicknesses, combined with inland penetration distances or area derived from aerial photos, to derive a volume of sediment (Morton and Sallenger, 2003). Others have used single or multiple pre- and post-overwash profiles multiplied by a unit width of barrier to arrive at deposit volume estimates (e.g. Schwartz, 1975; Leatherman, 1976; Fisher and Stauble, 1977; Leatherman, 1979a). These studies provide estimates of washover volume, but typically do not take into account the three-dimensional variability of the pre- and post-storm topography (Morton and Sallenger, 2003). In contrast, Kochel and Dolan (1986) installed a grid of colored sediment plugs across older washovers to determine the thickness of the subsequent deposits in the same area. They produced a contoured isopach map which accounted for spatially variable deposit thickness. Stockdon et al. (2007) also took the three-dimensional nature of deposits into account when determining their volumes by subtracting pre-overwash from post-overwash LiDAR topography data in order to arrive at a volume of sediment that was deposited over a large region that included a washover. The normalized volume values of washover deposits are typically tens of m^3/m (Table 1.). Volumes greater than 100 m^3/m are uncommon and are associated with confined overwash flows constricted laterally by high topography or channelization.

Table 1
Previous estimates of washover volumes normalized per shore-parallel length of washover. Intensities are given according to the Safar Simpson scale with TS = tropical storm; UR = unreported, CF = confined flow.
Expanded from Morton and Sallenger (2003).

Washover location	Storm	Intensity	Surge	Length	Thickness	Est. vol.	Data source
			(m)	(m)	(m)	(m^3/m)	
Miami Beach, FL	Hurricane 1926	4	3.2	180	0.3	54[a]	Reardon (1926)
Long Island, NY	Hurricane 1938	3	~3.6	75–90	0.9	~70–80[a]	Howard (1939) and Redfield and Miller (1957)
Long Island, NY	Hurricane 1938	3	~3.6	60	0.9	~54[a]	Wilby et al. (1939) and Redfield and Miller (1957)
Weekapaug Beach, RI	Hurricane 1938	3	~3.6	200	0.6	~120[a]	Nichols and Marston (1939) and Redfield and Miller (1957)
Charlestown Beach, RI	Hurricane 1938	3	~3	170	0.5	~85[a]	Brown (1939) and Redfield and Miller (1957)
Matunuck, RI	Hurricane 1939	3	~3	359	0.1	~35	Donnelly et al. (2001a)
Bolivar Peninsula, TX	Carla 1961	4	3	78	1.2	94	Morton and Sallenger (2003)
Matagorda Peninsula, TX	Carla 1961	4	4	750	0.25	CF 225	Morton and Sallenger (2003)
Ocean City, MD	Northeaster 1962	5	2.1	110	1.5	CF 165	U.S. Army Corps of Engineers (1963)
Core Banks, NC	Ginger 1971	1	1.2	100	0.1–0.3	10–30	Dolan and Godfrey (1973) and Simpson and Hope (1971)
Assateague Island, MD	Gilda 1973	TS	UR	UR	UR	5.5	Fisher et al. (1974)
Assateague Island, MD	Northeaster 1973	UR	~1	UR	UR	4.7	Fisher et al. (1974)
Outer Banks, NC	Northeaster 1973	UR	UR	~113000	UR	~12	Schwartz (1975)
Assateague Island, MD	Northeaster 1974	UR	~1	13	UR	20[b]	Leatherman et al. (1977)
Assateague Island, MD	Northeaster 1974	UR	0.8	UR	UR	28[b]	Leatherman (1976)
Assateague Island, MD	Northeaster 1974	UR	0.8	UR	UR	14[b]	Leatherman (1976)
Assateague Island, MD	Northeaster 1975	UR	1	UR	UR	2.7[b]	Leatherman (1976)
Assateague Island, MD	Northeaster 1974	UR	0.8	UR	UR	8.5[b]	Leatherman (1976)
Assateague Island, MD	Belle 1976	1	0.3	UR	~0.5	19[b]	Fisher and Stauble (1977)
Cape Cod, MA	Northeaster 1978	1	1.2	125	1.2	CF 150[b]	Leatherman and Zaremba (1987)
Nauset Spit, MA	Northeaster 1978	1	UR	UR	1.7	CF 102	Leatherman (1979b)
Assateague Island, MD	Northeaster 1982	UR	UR	~10–15	0.08–0.16	~13–28	Kochel and Dolan (1986)
Galveston Island, TX	Alicia 1983	3	3.8	30	0.7	21	Morton and Paine (1985)
Garden City, SC	Hugo 1989	4	3.6	70	0.5	35	Nelson (1991)
Debidue Beach, SC	Hugo 1989	4	UR	UR	UR	20–40	Eiser and Birkemeier (1991)
Martha's Vineyard, MA	Bob 1991	2	1.7	110–150	1.4–1.6	150–190	This study
Martha's Vineyard, MA	Northeaster Jan 1997	UR	~1	205	1.0	120[b]	This study
Cozumel, Mexico	Gilbert 1998	4	UR	40	0.7	28	Morton and Sallenger (2003)
Onslow Bay, NC	Bonnie 1998	2	1.7	UR	UR	23.9	Stockdon et al. (2007)
Onslow Bay, NC	Floyd 1999	4	2.2	UR	UR	29.3	Stockdon et al. (2007)

[a] Landward penetration distance of washover is estimated.
[b] Data from a single fan.

2. Study area

South Beach is a 25-km-long barrier located on the south-facing coast of Martha's Vineyard, a glacially-derived island located ~8 km south of Cape Cod, Massachusetts, USA (Fig. 2). The island is composed almost entirely of large terminal moraines and glacial outwash deposited predominantly during the last (Wisconsinan or Marine Isotope Stage 2) glaciation (Oldale, 1982). Central and southern Martha's Vineyard is composed of an expansive outwash plain that formed during local stagnation and retreat of the ice sheet lobes (Oldale, 1982). This outwash plain is composed of stratified sand and gravel deposits and contains numerous long north–south trending ponds (Woodworth and Wigglesworth, 1934). The barriers forming South Beach originally were thought to have formed offshore and migrated landward due to sea-level rise until they came in contact with the headlands of the drowned valleys (Woodworth and Wigglesworth, 1934). FitzGerald (1993) hypothesized that sediment eroded from the headlands between the bays would have provided material for the growth of spits across the mouths. Then, as sea-level rise continued, these spits migrated onshore, reducing the bay tidal prisms until inlets could no longer be maintained, and the continuous expanse of South Beach developed. The small bay areas, low tidal range, and strong longshore currents make inlets on South Beach ephemeral (FitzGerald et al., 1994) indicating that overwash processes must be the dominant mechanism for sediment to reach the backbarrier.

Modern South Beach is backed by one saline bay (Katama Bay), two large brackish ponds (Tisbury and Edgartown Great Ponds) and numerous small salt- and fresh-water ponds. Ephemeral inlets form at the openings to the larger ponds, occasionally disrupting the otherwise continuous stretch of South Beach. These inlets are generally formed in response to storms with the exception of an anthropogenic inlet on the eastern side of the barrier fronting Edgartown Great Pond (Fig. 2). For 11 years between 1997 and 2008, this inlet was opened an average of 2.5 times per year and remained open for an average of 12.5 days to allow for the maintenance of salinities and nutrient levels necessary to facilitate shellfish production in the pond (pers. com. William Wilcox, 2011).

The south shore of Martha's Vineyard is a mixed energy, wave-dominated (Hayes, 1979), microtidal (mean tidal range: 0.6 m; NOAA, 2010) coast. The shoreface (extending to the barrier toe) dips at an angle of ~1° to a depth of ~10 m (Cheung et al., 2007), then decreases to ~0.1° offshore to at least 20 m contour. Waves are dominantly from the south, which sets up an easterly longshore current on South Beach (up to ~0.5 m/s; Ogden, 1974). Sediment eroded from South Beach is carried by this current and deposited southeast of Chappaquiddick to form Wasque Shoal and the ephemeral Skiff's Island (Ogden, 1974). As expected from the large amount of sediment deposited to form the shoal, South Beach has undergone high rates of erosion. Average retreat rates for the south shores of Martha's Vineyard and Nantucket over the past two centuries are 1.4 m/yr (Hapke et al., 2010).

South Beach is open directly to the Atlantic Ocean and is therefore very susceptible to the impacts of large storms. Since 1848 there have been 88 tropical storms and hurricanes to pass within 150 km of Martha's Vineyard. Of these, only 8 have been category 4 or higher, 53 were between categories 1 and 3, and 27 were tropical storms (Knapp et al., 2010). Strong northeast storms (nor'easters) also greatly impact New England, typically between October and April. Currently, 10–11 strong nor'easters (winds in excess of 45 kt) impact New England each winter (Frumhoff et al., 2007). It is both of these storm types that cause the overwash along South Beach. This study examines washover fan deposits located in three ponds backing South Beach: Big Homer's Pond, Long Cove Pond, and Edgartown Great Pond (Fig. 2, Table 2).

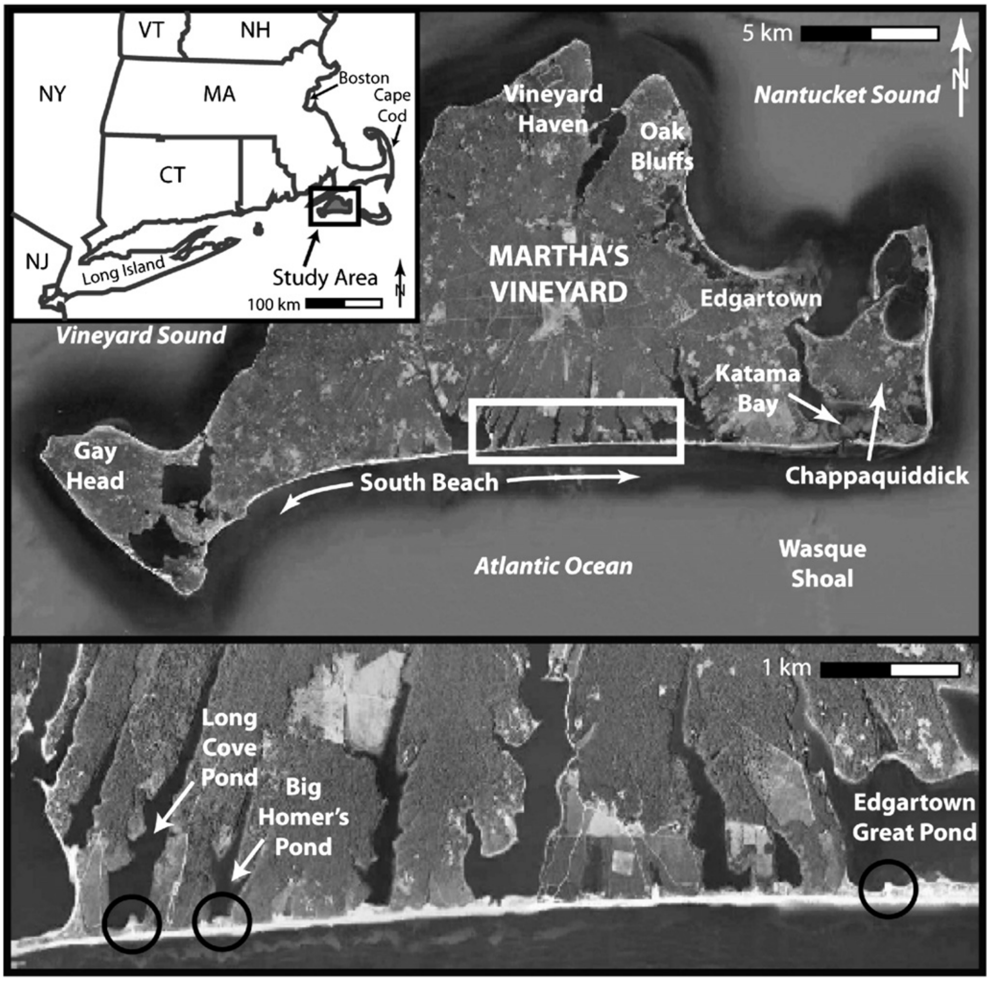

Fig. 2. Location map of study area on Martha's Vineyard, MA. The location is indicated by the black box in the inset. Bottom figure shows zoomed-in area indicated by the white box in the top figure. The three ponds of interest are indicated in the bottom figure with the washovers at each pond indicated by the black circles.
Top figure is modified from Google Earth™ and bottom figure is modified from 2008 orthophotos from MassGIS.

3. Methods

3.1. Field methods

Three washover fans were identified on the south shore of Martha's Vineyard from aerial photographs. The field investigation of these fans consisted primarily of coring, ground penetrating radar measurements (GPR), and differential global positioning system (dGPS) surveys (Fig. 3). Most field work was conducted in early August of 2009, with return trips to extend spatial coverage of data in July and September of 2010.

A total of 35 vibracores were collected in each pond (using a standard vibracore system from a floating raft) in a radiating grid pattern. Due to the sandy nature of the subsurface, the cores were fairly short, ranging from 39 to 301 cm with an average core length of about 130 cm. All of the sediment cores were visually described for macro structure, color, and grain size. Color descriptions were made using Munsell color standards (Munsell, 2000) and bulk grain size was determined by comparing samples with known standards at 10× magnification. In addition, all cores were scanned using an ITRAX XRF core scanner for radiographic images (step size 200 μm).

GPR was taken on the subaerial portion of each fan using a Malå Geoscience 250 MHz antenna (transmitter and receiving antenna within a single housing), with some lines taken with 500 and 800 MHz antennae at Edgartown Great Pond. GPR was also collected with the 250 MHz antenna floating on an inflatable raft on Big Homer's Pond and Long Cove Pond. All GPR data taken on land were distance-triggered with a wheel, while those taken in the ponds were time-triggered. A total of almost 5000 m of GPR profile was taken on land at Edgartown Great Pond, >600 m at Long Cove Pond, and >900 m at Big Homer's Pond. More than 11,000 m of GPR data were taken through the water column at Long Cove Pond and >5000 m was taken at Big Homer's Pond. This technique provided excellent bathymetry throughout the two ponds, as well as

Table 2
Comparison of Big Homer's Pond, Long Cove Pond, and Edgartown Great Pond.

	Big Homer's Pond	Long Cove Pond	Edgartown Great Pond
Approx. pond area	154,000 m^2	320,000 m^2	3,400,000 m^2
Fronting barrier length	220 m	340 m	2400 m
Highest elevation on barrier	4.29 m	5.06 m	5.61 m[a]
Lowest elevation on barrier	2.55 m	1.66 m	1.66 m[a]
Approx. barrier width[b]	75 m	75 m	105 m
Maximum pond depth	−2.7 m	−3.5 m	−5.0 m[c]
Number of inlets	0	0	1 (temporary)
Anthropogenic use	Some	Heavy	Some

[a] Section of barrier near fan of interest.
[b] Widths are of areas not containing washovers.
[c] Behind section of barrier containing fan of interest.

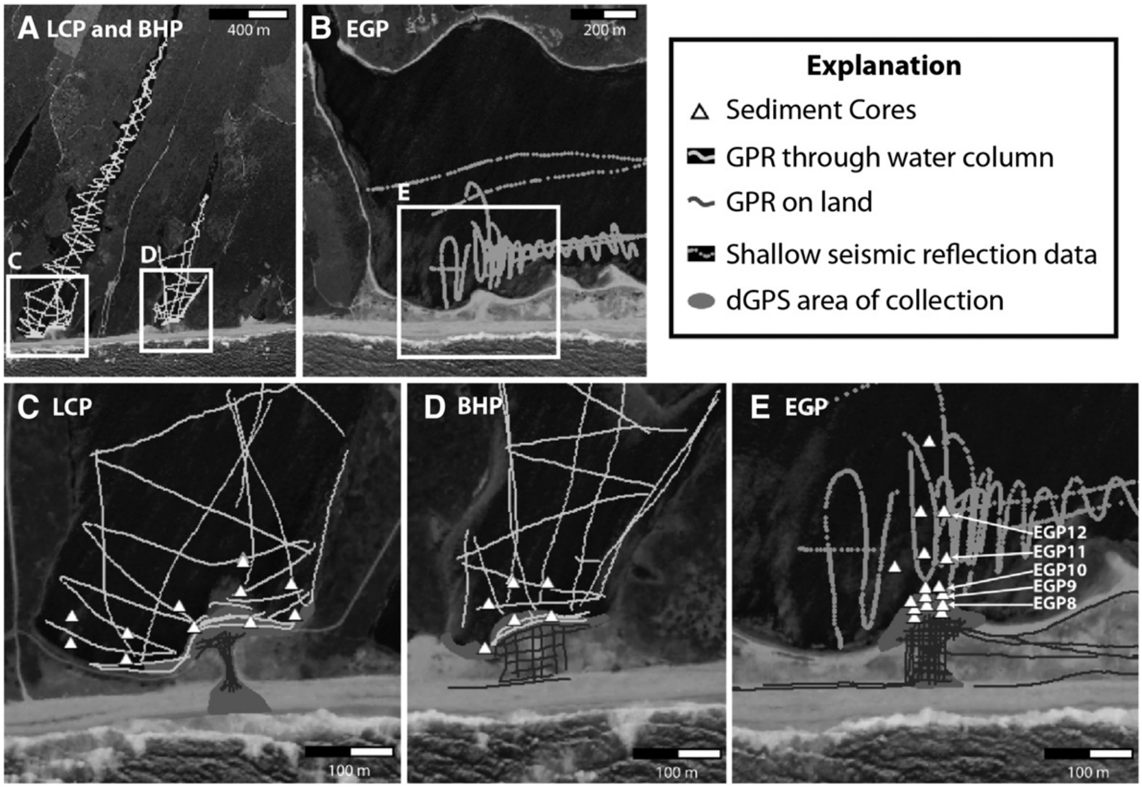

Fig. 3. Data collected at each pond. A depicts Long Cove Pond to the left and Big Homer's Pond to the right. Boxes indicate locations of C and D. B depicts the washover at Edgartown Great Pond with a box to indicate the location of E. C, D, and E show the dense data collected proximal to and on each washover at Long Cove, Big Homer's, and Edgartown Great Pond, respectively. Note that C, D, and E all have the same scale. Cores labeled in E are those included in transect in Fig. 5.
Images are modified from 2008 orthophotos from MassGIS.

sub-bottom structure in shallow water, penetrating to a depth of about 4–6 m. Unfortunately, this method was not possible in Edgartown Great Pond due to its comparatively high salt water concentration. Penetration was also poor (~1 m) on the subaerial portion of this fan, likely due to the shallow salt water table. Instead, bathymetry at Edgartown Great Pond was determined acoustically using >3000 m of seismic data collected using a 10 KHz SyQuest StrataBox. Some internal structure of the fan was revealed by the excavation of an ~20 m long, up to ~1 m deep trench.

Modern surface morphologies of the fans were determined by taking dGPS surveys using a Trimble ProXRT with real-time corrections from OmniSTAR. The surveys had maximum vertical errors of between 10 and 30 cm and lateral positioning errors on the order of 10 cm. The surveys were taken on the subaerial portions of the fan as well as in the water, to bridge the data gap between the bathymetry provided by the GPR and Stratabox data and the topography available with LiDAR (JALBTCX, 2009). Spatial resolution of dGPS data was variable as the data were logged at about 1 s intervals, though a maximum of roughly 1–3 m spacing was achieved for the almost 9000 data points.

3.2. Data processing

GPR data were processed using DECO-Geophysical Ltd.'s RadExplorer software package. Processing typically included DC (mean) removal, time-zero adjustment, background removal, 2D spatial filtering, predictive deconvolution, amplitude correction using automatic gain control, band pass filtering, Stolt F-K migration, and topographic correction. The topographic corrections were performed using LiDAR data or dGPS data, depending on the quality of the dGPS data which was affected by satellite geometry and periodic antenna obstruction. Time varying velocity models were constructed for data collected in the ponds with a velocity of 3.33 cm/ns used for the fresh water and 6.0 cm/ns used for the sediment. Although diffraction hyperbolas occurred infrequently in the data, this sediment velocity was based on hyperbolic velocity analysis of those that were found and applied to all saturated sediment. Reflections corresponding with surfaces of interest were picked in RadExplorer using a combination of manual and auto-fill parameters.

The Stratabox data were post-processed using Triton Imaging, Inc.'s SB-Interpreter software. Processing procedures were similar to those used to process GPR data and include flat and time-varying gain adjustment, bandpass filtering, and vertical downsampling. The sediment–water interface was picked manually.

After post processing was complete, 3D locations and other spatially varying information (e.g., GPR trace numbers, dGPS accuracy) of all data were spatially analyzed in ArcMap. The geospatial reference frame of all the data collected was set to the Universal Transverse Mercator (UTM) coordinate system with the WGS84 ellipsoid, using Data East's XToolsPro extension for ArcMap. Standard offsets between the different vertical datums (pond surface, dGPS, and LiDAR) were determined by comparing as many overlapping points as possible (typically 15 to 50) and all data was vertically referenced to the water level in each pond.

3.3. Three dimensional surface calculations

Two surfaces were created using universal kriging for each pond: a modern surface and a pre-overwash surface. Surfaces were kriged using Golden Software's Surfer8 program. The modern surfaces were kriged with data from GPR (Stratabox at Edgartown Great Pond), LiDAR, dGPS, and pond outlines picked from orthophotos in ArcMap. Pre-overwash surfaces were kriged with data from cores, GPR whenever possible, and a zero elevation contour on all but the southern sides of the pond taken to be the location of the pond edge as determined from orthophotos.

Pre-overwash surfaces were subtracted from the modern surfaces to create isopach maps of the washovers. Ideally, beyond the extent of the washover, the pre-overwash and modern surfaces would be the same. Unfortunately, due to limited sediment core data coverage, the farthest landward extents of the washovers were not captured. Thus, the pre-overwash data includes a zero elevation contour at the distal pond edge as it is assumed that the washover did not extend past the edges of the pond. Consequently, the zero elevation contour causes the estimated pre-overwash surface to rise above the elevation of the modern surface past the extent of the washover because of the lack of data between the two regions (the washover and the zero elevation contour). This difference results in the negative points in the isopach map that mark the edge of the washover. These negative points are beyond the extent of the data coverage and were therefore discarded. The volume under the resulting map of the washover is then determined by numerical integration.

4. Results

4.1. General

The three ponds of interest to this study all display similar results. GPR data collected through the water column at Big Homer's and Long Cove Ponds show weak reflectivity with the exception of one strong reflector seen at varying depths (Fig. 4A). Where this reflector is shallow (less than about 3 m depth), some underlying reflectors are visible. In contrast, GPR profiles collected both in shallow water (especially proximal to the fan) and terrestrially extend to a maximum of ~8 m, depending on the transmitted frequency.

The combination of radar and sediment core data allows us to define a series of four sedimentologic units labeled A–D, from bottom to top (example stratigraphy and GPR data typical of all three ponds shown in Figs. 4 and 5). Unit A is recognized in 19 cores as layers of coarse sand (0.5–224 cm thick) interbedded with one to 18 beds of either mud (1–113 cm thick) or occasional peat or shell hash. This unit is not visible in GPR profiles due to signal attenuation. Unit B is present in 17 cores and ranges in thickness from 1 to 103 cm. It is composed of massive silty clay with occasional flecks of decomposing organics. The GPR signal attenuates quickly in Unit B, a characteristic common to muddy environments due to the high conductivity of clay (Baker et al., 2007). Although little structure is evident in this GPR unit, any visible internal reflectors are generally horizontal. This unit typically has a sharp upper contact with Unit C in the cores, which is seen as a very strong reflector in the GPR profiles (Fig. 4B, C). Unit C is seen in 29 cores and is composed of a poorly sorted, coarse to very coarse sand. This unit is generally massive, contains few heavy minerals, and varies from 3 to >126 cm thick in the cores, thickening southward toward the barrier to reach a maximum of ~450 cm thick in the radar sections. In lines collected along north-to-south, shore-normal, profiles, Unit C contains internal reflectors that dip northward into the pond (Fig. 4B). These reflectors have a sigmoidal shape as they shoal toward the top of the unit from 5 to 10° near the bottom, to 1 to 5°, to top reflectors nearly horizontal at <1°. Internal reflectors in this unit in profiles collected along east/west, shore-parallel lines have an approximately Gaussian- or bell-like shape (Fig. 4C): they are nearly horizontal (<1°) at the center and then dip to both sides at 5–15° before becoming nearly horizontal distal to the center of the structure. Though not distinguishable from the top of Unit C in GPR, five of the cores are topped by a thin (<0.5–3 cm) Unit D of saturated mud.

4.2. Big Homer's Pond

Seven cores were collected at Big Homer's Pond ranging in length from 60 to 260 cm long. Unit A is recognized in four cores as layers of coarse sand (51–224 cm thick) interbedded with one to five beds of either mud (3–9 cm thick) or occasional peat (12 cm). Unit B is present in five cores and ranges in thickness from 29 to 103 cm. It is composed of massive, very dark gray (2.5Y3/1; Munsell, 2000) silty clay with occasional flecks of decomposing organics. Unit C is composed of an olive brown (2.5Y4/4), poorly sorted, coarse to very coarse sand. This unit is generally massive, contains few heavy minerals, and varies from 14 to >126 cm thick in the cores, thickening southward toward the barrier to reach a maximum of ~450 cm thick in the radar sections. Two of the cores are topped by a thin (1–2 cm) Unit D of very dark grayish brown (2.5Y3/2) saturated mud.

4.3. Long Cove Pond

Twelve vibracores were collected at Long Cove Pond ranging in length from 39 to 301 cm. Unit A was seen in eight of the cores. Cores contain 1–18 beds in this unit, with 0.5–114-cm thick sand beds, 3–113-cm thick mud beds, and one instance each of solitary beds of mixed shell hash (19 cm thick) and peat (4.5 cm thick). Unit B is identified clearly in four cores. It is a massive very dark brown (10YR2/2) silty clay, 1 to >56 cm thick. When visible in radargrams, Unit B contains horizontal reflectors, though there is little signal penetration into the unit (Fig. 4). Seven cores contain the massive olive brown (2.5Y4/3) coarse sand typical of Unit C. This unit is 3 to >107 cm thick, increasing toward the south. Radar profiles indicate that Unit C reaches a maximum depth of ~450 cm at the southern edge of the fan. Shore-parallel radar profiles show an asymmetry in the thickness of the unit, with the thickest regions on the western side of the fan. The internal structure is seen as reflectors with Gaussian-like shapes, though the shape demonstrates a marked easterly skewness with much steeper maximum dip angles on the western side (~20°) than on the eastern side (~4°). Internal reflectors are more chaotic than at Big Homer's Pond. In three of the cores, Unit C is overlain by the very dark grayish brown (2.5Y3/2) saturated mud of Unit D, ranging from a thin lens (<0.5 cm) to 3 cm thick. In four cores, Unit C is not present and Unit B grades directly to Unit D. The combined thickness of Units D and B in these cores is 2–18 cm.

4.4. Edgartown Great Pond

Sixteen vibracores were collected at Edgartown Great Pond, ranging from 48 to 158 cm in length. Due to the brackish water in this pond, maximum GPR penetration is only ~150 cm, and typically less than 100 cm. A shore-normal trench provided some insight into the top ~70 cm of the subaerial portion of the fan. Shallow seismic reflection profiles were used to map pond bathymetry. However, shallow multiples and a low signal to noise ratio prevented interpretation of subbottom data.

Unit A is identified in seven cores with 1–5 beds present containing sand layers ranging from 1.5 to 122 cm thick with occasional mixed shell hash and mud layers ranging from 1 to 8 cm thick. Eight cores contain the dark olive brown (2.5Y3/3) silty mud common to Unit B. These layers are 2 to >15.5 cm thick. One core contained shell hash mixed into this unit. Unit C is identified in 15 cores as a coarse to very coarse, light olive brown (2.5Y5/3) sand, 93–124 cm thick. Several cores contained shell fragments and pebbles in this unit. Unit C is identified in GPR profiles as a series of shallowly (<2°) northward dipping clinoforms. The bottom contact between Units B and C is not seen in the radargrams and only the top of Unit C is captured due to signal attenuation. The trench displays similar shallowly northward-dipping layers corresponding to those seen in radar reflectors. Only two cores contain the olive gray (5Y4/2) mud of Unit D, in one of these Unit C is absent so Unit B grades directly into Unit D. Here, these two units have a combined thickness of 11 cm.

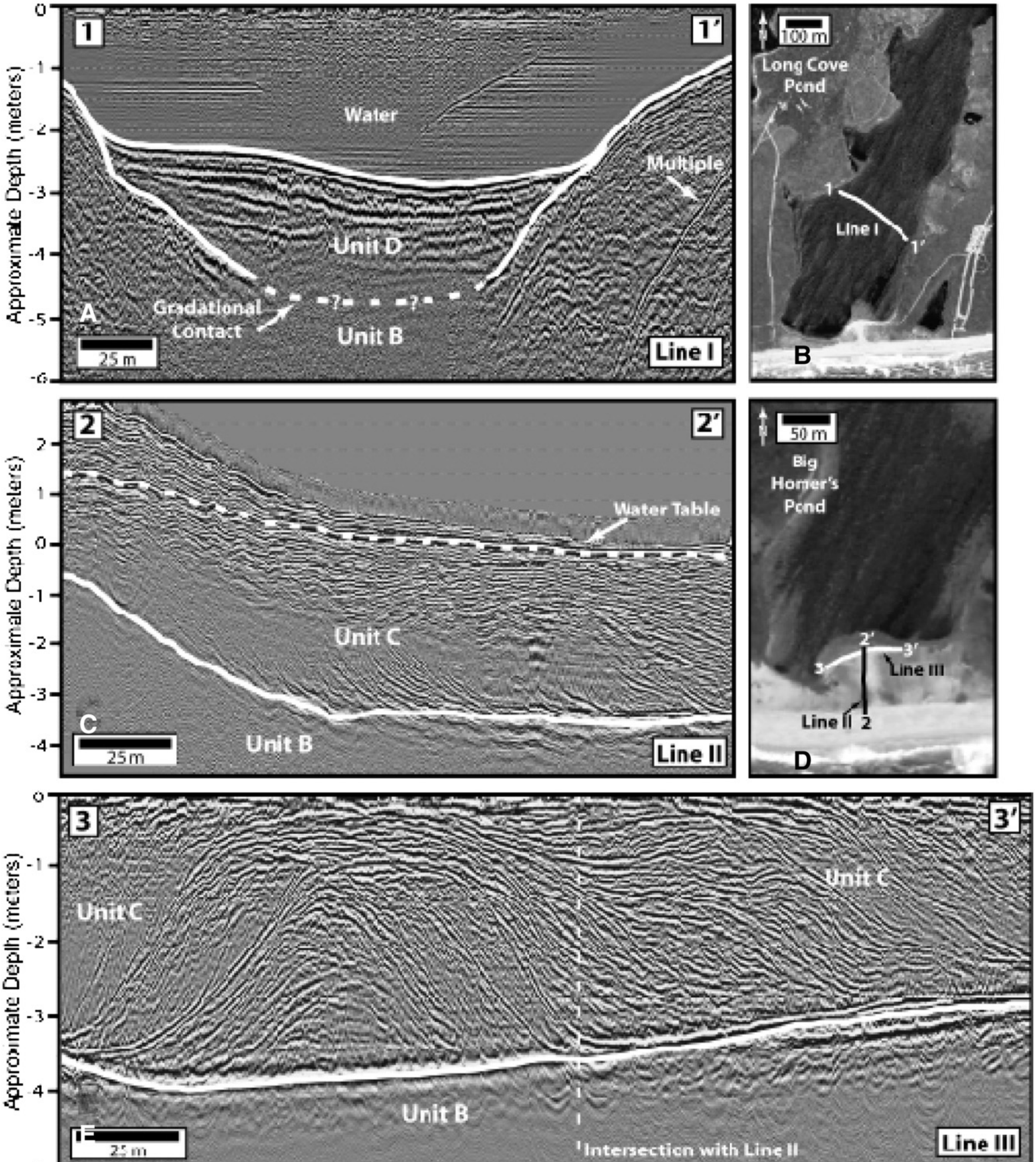

Fig. 4. GPR profiles with sedimentary units identified. Vertical scale is referenced to each pond's still water level. Box A: radargram from Long Cove Pond (location of line is indicated in box B) taken through the water column. Box C is a radargram from Big Homer's Pond taken on land and topographically corrected. Location of line is given in Box D. Box E is a radargram from Big Homer's Pond taken on land and topographically corrected (profile is flat). Location of line is given in box D.

5. Interpretation and discussion

5.1. Part I: interpretation of stratigraphy, calculation of washover volumes and sediment fluxes

The first step towards estimating onshore sediment flux caused by major storms, is to estimate the volumes of specific deposits. In calculating these volumes, this study considers the three-dimensional pre- and post-storm morphologies of the topographically low, southward-facing barriers of the southern coast of Martha's Vineyard, MA. The second step is to estimate the recurrence intervals for storm events causing similar magnitudes of overwash so that a sediment flux across the barrier can be estimated. The fans described above were deposited in historic times by known storms (path and magnitude). This allows the use of meteorological and tide gauge data to estimate recurrence intervals of the surges that caused the deposits. These recurrence interval

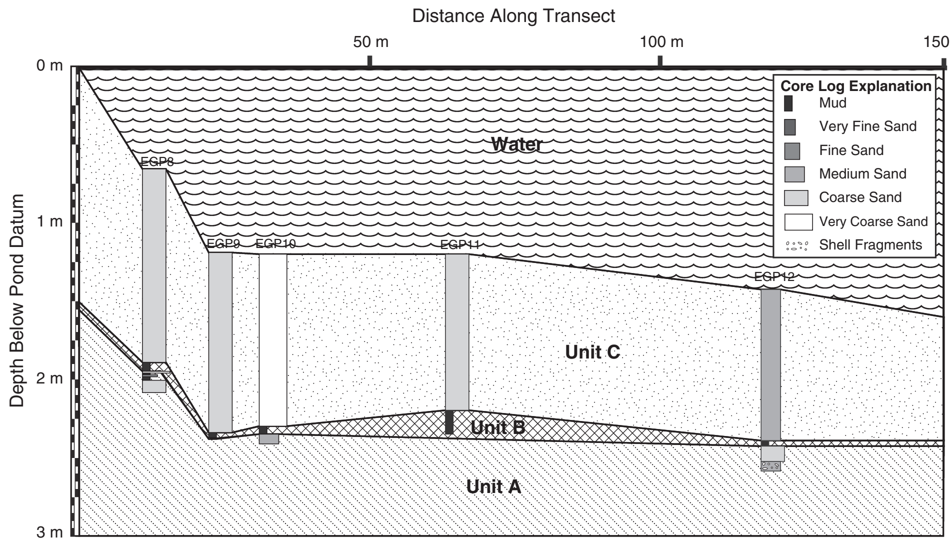

Fig. 5. Stratigraphic section of five cores from Edgartown Great Pond showing Units A though C. Cores used in the profile are labeled in Fig. 3. The distance along transect goes from south (0 m) to north (150 m).

estimates, combined with the volume of sediment transported, allows for a first-order estimate of the onshore flux of sediment from these overwash events to be calculated.

5.1.1. Interpretation of stratigraphic units

Stratigraphies interpreted from cores and radar data (Fig. 5) are similar across the ponds and are therefore interpreted to have resulted from the same processes. Unit A is interpreted to be sand deposited during earlier overwash events, interbedded with mud deposited in a quiescent lacustrine environment. Unit B represents mud deposited in the pond immediately prior to the deposition of the massive sands of Unit C. The sharp contact seen in cores and the strong reflector truncating underlying weak reflectors seen in radar images likely indicates a strongly erosional upper boundary created during the deposition of the overlying sediment. Unit C contains the sand of the washover deposit. We interpret the sigmoidal reflectors seen within the unit as clinoforms, which would suggest that the unit was first deposited in a small fan or tongue during the early stages of the overwash event. This fan then built laterally and vertically during the course of the overwash event, until a fan shape had developed. The steep reflectors near the bottom of the unit show the delta-like structure of the fan. The deposit thins distally to and along the barrier, and most sediment is deposited closer to the throat of the overwash fan. The thin sediment of Unit D is the modern pond mud.

5.1.2. Washover volumes

A few assumptions allow for the estimation of washover volumes from the detailed stratigraphic analyses at each of the three sites. First, the lower boundary of the deposit is taken to be the erosive contact between Units B (lacustrine mud) and C (washover sand). This surface is likely topographically lower than the actual pre-overwash surface, most likely due to scouring of the barrier and backbarrier pond during the initiation of the overwash event. Second, the portion of the washover that contributes to the landward migration of the barrier is taken as only that which is deposited landward of the pre-overwash barrier. This boundary is taken to be the vertical plane created by the vegetation line on either side of the washover (Fig. 6).

Isopach maps were created for the washovers in each of the three ponds (Fig. 6) by digitally subtracting the surface created for the lacustrine mud/washover boundary from the modern surface. Washover dimensions and volumes for each of the three ponds are given in Table 3. The three fans have similar volumes: the smallest (Big Homer's Pond) is only ~12% smaller than the largest (Edgartown Great Pond). The deposits at Big Homer's Pond and Long Cove Pond demonstrate similar surface areas. The deposit at Edgartown Great Pond covers a surface area 160–180% larger than the other two. However, it displays an average thickness of only 40–60%, as thick as the washovers in the other ponds, resulting in the similar washover volumes at all three ponds.

The assumptions made to infer washover volume result in several potential sources of error. The first assumption, that the lower boundary is taken as the erosive surface between Units B and C, does not correct for any scour that occurred during the overwash. It is assumed that this scoured sediment is largely worked into the washover, consistent with the somewhat poorly sorted base of Unit C. Such scour would cause the true B/C boundary to be lower than the actual pre-overwash surface. Taking the modern B/C contact as the pre-overwash topography results in larger volume estimates than the volume of sediment that was actually driven landward from the front of the barrier or offshore during the overwash event.

The second assumption, that the portion of the washover that contributed to the landward migration of the barrier is that landward of the vegetation line, assumes that a vertical plane truncates the seaward side of the washover deposit. This vertical plane ignores contributions from tapering of the deposit seaward. The washover deposits do pinch out; however, this occurs farther seaward towards the beach itself.

Another assumption is that any aeolian transport of sand that occurs concurrent with or following the storm is also included in volume calculation. This additional volume is not expected to greatly influence the volume calculation as the sediment found in the cores was not noticeably finer towards the top of Unit C as would be expected with sediment deposited by aeolian transport.

A final source of error in estimating washover volume is specific to Edgartown Great Pond. Inclusive in the washover isopach is a small lobe of sediment on the eastern side of the deposit that does not appear to originate from the washover of interest, likely resulting from poor data coverage in this region. As seen in orthophotos, this sediment is likely derived from reworking of adjacent older overwash fans by local wind waves in the pond (Fig. 6C), as further evidenced by the concavity of the isopach map along that side of the fan. This sediment was excluded from the volume calculation. The difference in the total washover volume resulting from this truncation is only 0.08×10^4 m^3, or ~3%.

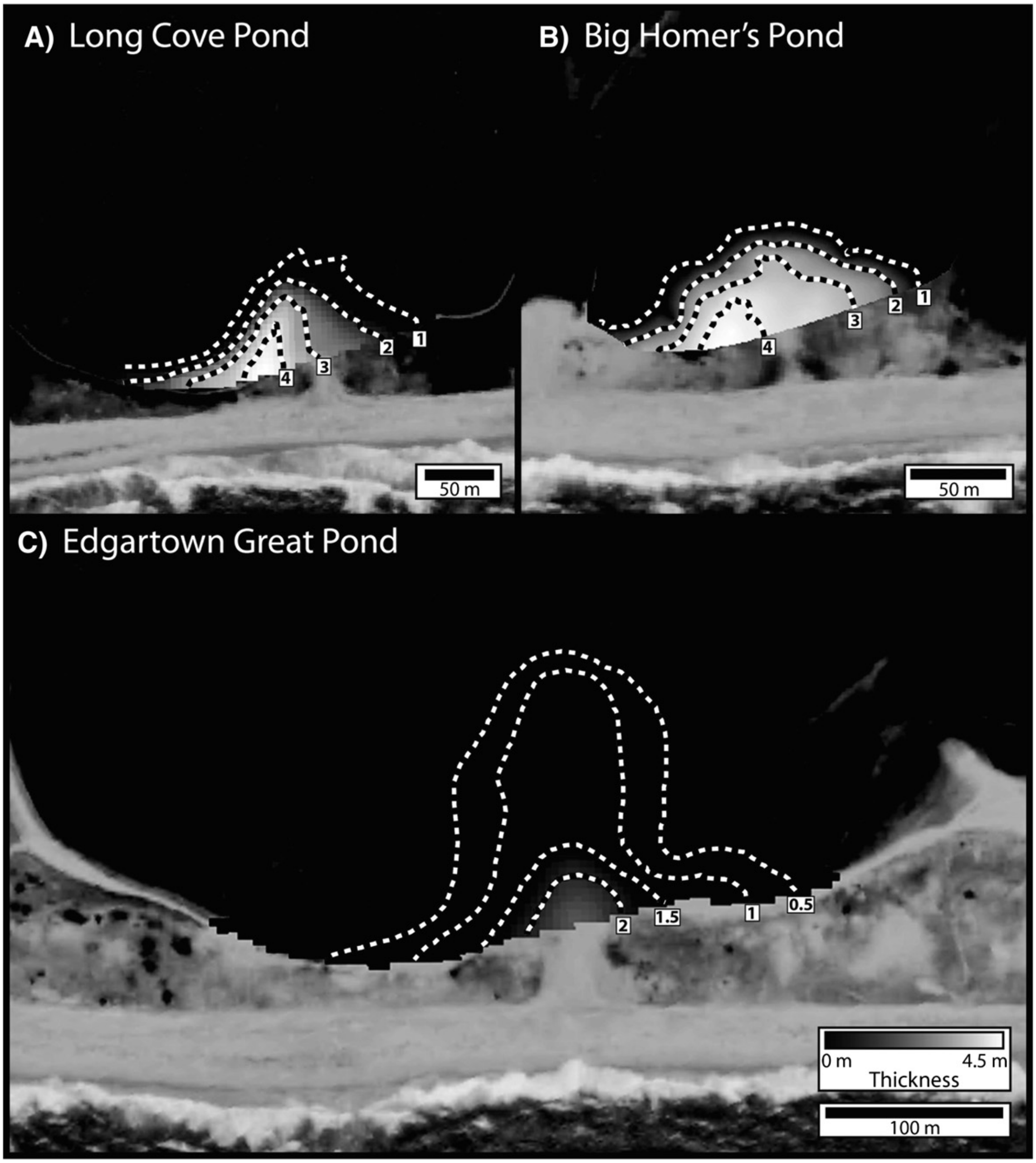

Fig. 6. A, B, C: isopach maps of the washovers from Big Homer's Pond, Long Cove Pond, and Edgartown Great Pond, respectively. Contour lines are indicated by the white and black hashed lines and are at 1 m intervals for A and B and at half meter intervals for C. Contour labels are in meters. The gray scale is the same for all three figures and is indicated in C. Note the older washover to the east of the washover of interest in C. Reworked sediment from this washover was excluded from the isopach seen here, as discussed in the text. Note also that the southern edges of the deposits follow the vegetation line, as discussed in the text.
Maps are overlaid on 2008 orthophotos from MassGIS.

5.1.3. Dating the washovers and correlated storms

The timing of the most recent overwash events in the study areas was determined using aerial photos. Cheung et al. (2007) used aerial photos from March 1991 and November 1992 to bracket the overwash events at Long Cove and Big Homer's Ponds to this period (Fig. 7). Hurricane records (specifically The Best Track Reanalysis Data from the National Oceanic and Atmospheric Administration's (NOAA) National Hurricane Center; Neumann et al., 1993; Landsea et al., 2004) and monthly maximum water levels from two nearby tide gauges (Newport, RI and Woods Hole, MA; NOAA, 2011a,b) were used to identify the storm that produced the maximum surge at the location of the fan during the time interval defined by the aerial photos. Hurricane Bob was the strongest storm during this time period, though the Halloween Eve Storm (the “Perfect Storm”) of 30 October 1991 occurred in the same period. The tide gauge at Woods Hole, MA indicates that the Halloween Eve Storm produced significant storm tides of 0.94 m above mean high water (m MHW; NOAA, 2011b). However, the water level from this nor'easter was not as high as the 1.50 m MHW on 19 August 1991

Table 3
Washover dimensions and volumes for each pond.

Pond	Volume	2D surface area	Maximum thickness	Average thickness
	(10^4 m^3)	(10^4 m^2)	(m)	(m)
Big Homer's Pond	2.1	1.5	4.5	1.4
Long Cove Pond	2.3	1.4	4.4	1.6
Edgartown Great Pond	2.4	2.5	2.5	1.0

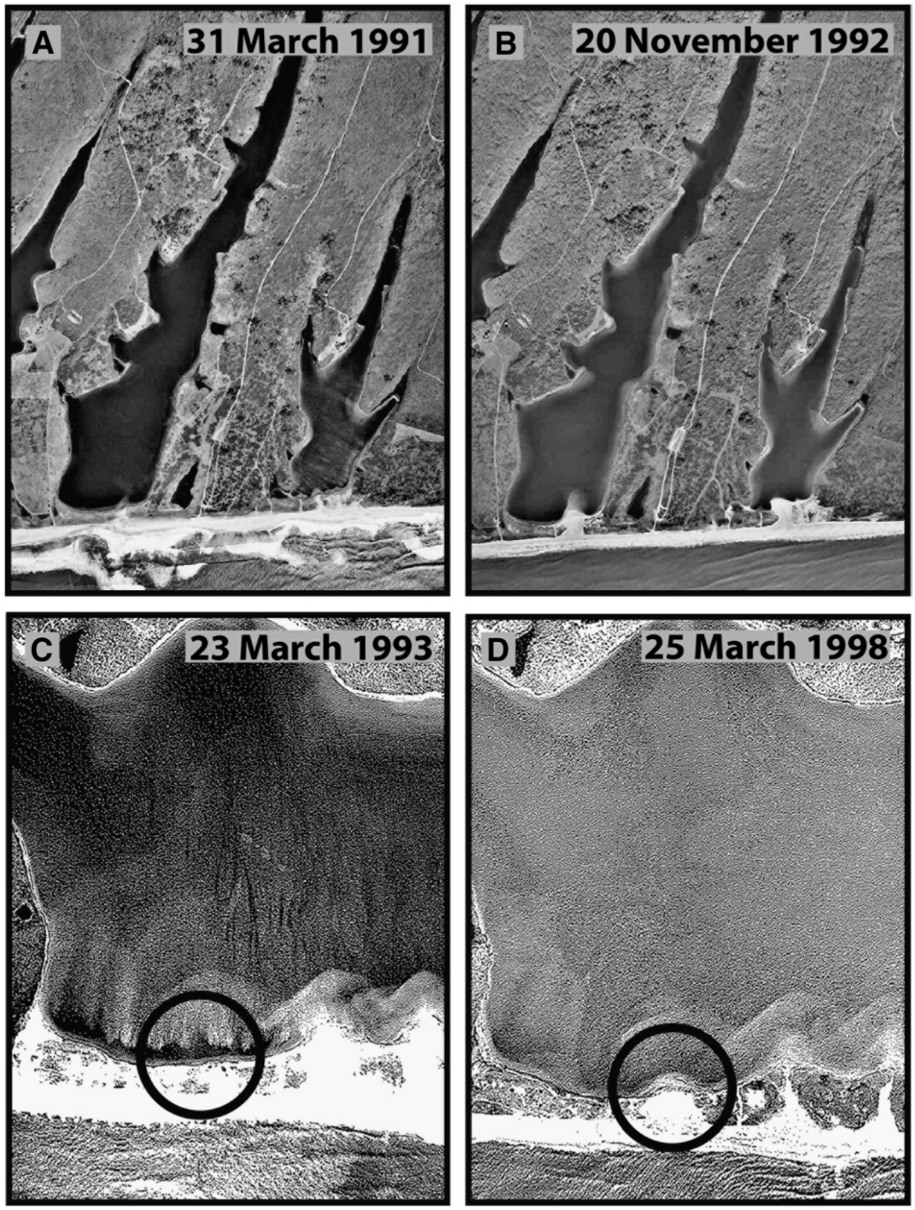

Fig. 7. Aerial photos bracketing the deposition of the washovers at Big Homer's and Long Cove Ponds (A and B) and at Edgartown Great Pond (C and D). Figure A is from 31 March 1991, B is from 20 November 1992, C is from 23 March 1993, and D is from 25 March 1998. Note in figures C and D that the washover of interest to this study is at the circled location.
Images in A and B are from Cheung et al., 2007 and images in (C) and (D) are from the James W. Sewall Co.

(NOAA, 2011b) produced by Hurricane Bob, which passed 50 km west of Martha's Vineyard, allowing its strongest winds to directly impact the southerly facing South Beach (Cheung et al., 2007). Hurricane Bob made landfall at Newport, Rhode Island as a category 2 storm with winds of 160 km h^{-1} (Fig. 8; Mayfield, 1992). The surge created by Hurricane Bob at Long Cove and Big Homer's Ponds was computed using the Sea, Lake, and Overland Surges from Hurricanes (SLOSH) model to give a maximum surge of 1.7 m (Jelesnianski et al., 1992; Cheung et al., 2007 report a maximum surge of about 1.45 m).

The most recent washover at Edgartown Great Pond was deposited later than those at the other ponds. Aerial photos bracket the overwash event between March 1993 and 1998. Tide gauges at Newport, RI and Woods Hole, MA indicate that the highest water level during this interval occurred during a nor'easter on 10 January 1997 with a storm tide of 0.95 m MHW at Woods Hole (NOAA, 2011b).

5.1.4. Recurrence interval of storm water levels

To determine the return intervals of storms with the characteristics of Hurricane Bob and the January 1997 nor'easter, we used the monthly extreme water levels from the Woods Hole tide gauge over the past ~73 years (NOAA station ID 8447930; NOAA, 2011b). The 90th percentile of the data (0.596 m MHW) was determined, and all smaller values were removed. Then, a generalized Pareto distribution (GPD) was fit to those data, using 0.596 as the value for theta (Lin et al., 2010). The fit was evaluated for between 0.6 and 3.6 m MHW at 10 cm intervals. There were 884 months of data with 77 values exceeding 0.6 m, so the average return time for water levels in the 90th percentile is ~1 year. The cumulative probability from the GPD fit was used to calculate the return intervals for each 10 cm bin of water levels (Fig. 8). The return interval for the water level associated with Hurricane Bob is ~28 years and that associated with the January

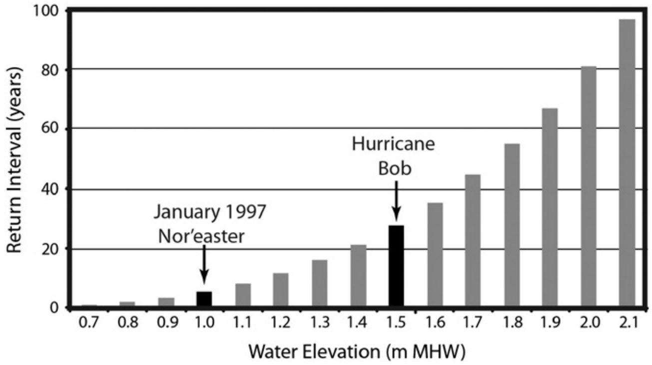

Fig. 8. Return intervals for water levels based on extreme value theory (generalized Pareto fit) applied to Woods Hole, MA tide gauge data. Labels on the horizontal axis are the central values of the 10 cm bins. The return interval for a water level greater to or equal to that produced by the January 1997 nor'easter is about 6 years and that produced by Hurricane Bob is about 28 years.

1997 nor'easter is ~6 years (Lane, 2011). The monthly nature of the tide gauge data means that only the highest water level is recorded each month, so lower water levels are likely underestimates. As the higher water levels are of interest to the study, only those values greater than 0.6 m were used in the fit and therefore this error should not greatly affect the estimated return intervals.

5.1.5. Overwash fluxes

Given the calculated washover volumes, V (m^3), the length of barrier affected by the overwash, L (m), and the return interval of the surge that created the deposit, T_S (yr), onshore width-normalized sediment fluxes, Q_{OW} (m^3/m/yr), for each of the three ponds is estimated as:

$$Q_{OW} = \frac{V}{L * T_S}. \tag{1}$$

The length of the affected barrier is defined as either the alongshore length of the barrier fronting the pond containing the washover if there are no other washovers in the pond, or the distance from the edge of the pond to half-way between the washover of interest and the neighboring washover if there are multiple washovers in a pond. Flux values are given in Table 4 based on the estimates of the return times of the storm tides that caused the overwash events. The volume per unit length of barrier is not the same as that given in Table 1 because the length used in Table 1 is the alongshore dimension of the washover fan itself, whereas the length presented in Table 4 is that of the affected section of barrier. The alongshore length of the fan and the length of the affected barrier are similar at Big Homer's and Long Cove Ponds. However, at Edgartown Great Pond, the barrier is much longer than the overwash fan. These flux calculations assume that the barrier overwashes if the water level is greater than or equal to the maximum water level that occurred during the storm that caused each overwash. If a storm does not produce a sufficiently high water level, then it is assumed that there is no onshore sediment flux. This approach allows complex processes, including wave run-up, and barrier geometries (including barrier height) to be taken into account implicitly because they are included in the high water level values.

Despite the similarity in the volumes of the washovers calculated at the three ponds, the ranges of flux estimates highlight the differences in affected barrier length and water elevation return interval. The flux is highest at Edgartown Great Pond due to the short return time of the water level needed to overtop the barrier. This suggests that there may be a typical, or maximum volume that is deposited as washover once a certain threshold of water elevation is met, at least for the specific range of offshore and barrier morphologies encountered in this study. Therefore, onshore sediment flux is maximized when an overwash is caused by the smallest necessary water level: these will have much smaller return intervals than the larger storms that produce a similar volume of washover. This contradicts the findings of Kochel and Dolan (1986), who found that larger storms contribute more to overwash flux than smaller frequent storms on southern Assateague Island, MD. This could indicate that there may be a threshold of water level needed to produce the "typical" washover volume and that very small overwash events will not reach this threshold, though future work is needed to expand the data set to verify this suggestion.

Table 4
Overwash fluxes and associated parameters.

	Big Homer's Pond	Long Cove Pond	Edgartown Great Pond
Washover volume	2.1×10^4 m^3	2.3×10^4 m^3	2.4×10^4 m^3
Affected barrier length	220 m	340 m	470 m
Return time	28 yr	28 yr	6 yr
Vol./affected barrier length	96 m^3/m	68 m^3/m	51 m^3/m
Onshore sediment flux	3.4 m^3/m/yr	2.4 m^3/m/yr	8.5 m^3/m/yr

5.2. Part II: implications

5.2.1. Comparison with previous work

The overwash volumes calculated for the three South Beach washover fans range from 120 to 190 m^3/m. These values are higher than most of those reported previously (Table 1) and typically coincide with values of washovers deposited by a confined flow (i.e., when the throat of the washover is constricted by high topography so the overwash is channeled through a small opening). The washovers of interest here all have a distinct throat, narrower than the rest of the deposit, so they could be considered confined flow. However, there is no hard structure confining the overwash; rather, they are bounded by erodible aeolian dunes. Alternatively, the high values from this study could indicate the importance of recognizing the three-dimensional nature of the deposit—not doing so appears to result in an underestimate of the normalized washover volumes. Additional work would be necessary to measure the three-dimensional volume of a washover at a location where pre- and post-overwash profiles have been conducted in order to determine if similar values are measured using each method.

5.2.2. Implications for long-term barrier evolution

The south shore of Martha's Vineyard has been retreating at a rate of about 1.4 m/yr over the last ~200 years (Hapke et al., 2010). In a simple geometric model of barrier transgression, a barrier is able to maintain its form and migrate landward if it overwashes at a rate defined by its geometric constraints, Q_{OW^*} (Fig. 9). Using a priori information about the barrier geometry (pond depth, D_P, barrier height, H_B, and barrier toe depth, $D_{BT} = -10$ m; presented in Table 2) and shoreline retreat rate, R_S, this equilibrium flux can be estimated from Eq. (2) and the amount of sediment eroded from the shoreface, Q_{SF}, can be estimated from Eq. (3) assuming that sediment is eroded evenly from the entire shoreface.

$$Q_{OW^*} = (D_P + H_B) * R_S \tag{2}$$

$$Q_{SF} = (H_B + D_{BT}) * R_S. \tag{3}$$

Table 5 contains the fluxes necessary to maintain a stable barrier at each pond using the range of barrier heights at each pond as well as an estimated flux of sediment eroded from the shoreface. The overwash flux necessary for the barrier to maintain a stable shape averaged over the three ponds is ~10 m^3/m/yr. This flux is about half of the material removed from the shoreface, ~19 m^3/m/yr, using the shoreface depth to the barrier toe of ~−10 m. The other material removed from the shoreface is likely removed due to gradients in alongshore transport, although it could potentially be permanently transported offshore during storms. This excess volume lost from the shoreface could conceivably also be deposited as washover and actually cause the barrier to widen. The actual onshore sediment flux due to overwash estimated here is less than the value needed to maintain the barrier in its current shape (Fig. 9; see Tables 4 and 5 for values), although values are within an order of magnitude and the high end of the range in fluxes calculated at Edgartown Great Pond approaches this value. Aeolian processes could also contribute to the onshore flux of sediment; as such fluxes would be included in the deposits we measure, the presence of significant aeolian transport would only reduce the estimate of overwash flux.

The low sediment flux from overwash calculated here suggests that South Beach is not in steady state and is thinning. This interpretation is consistent with orthophotos which show that the barrier width near the three fans studied here has decreased by ~15 m between 1994 and 2008, equivalent to a decrease in barrier width of ~1.1 m/yr. This value suggests that only ~24% (or about 2.4 m^3/m/yr) of the onshore sediment flux needed to maintain the retreating barrier is occurring, a number remarkably similar to the fluxes calculated at Long Cove and Big Homer's Ponds (2.4 and 3.4 m^3/m/yr, respectively), but smaller than that calculated at Edgartown Great Pond (8.5 m^3/m/yr). Leatherman (1979a,b) suggests that overwash is infrequent until a barrier thins to a critical barrier width, after which point overwash increases and the barrier is able to migrate onshore. Accelerated sea-level rise and increased storm intensities and/or frequencies could prove beneficial to South Beach as these factors will likely increase the frequency of overwash. Relative sea-level rise would also decrease the magnitude of the surge needed for the barrier to overwash. These factors would allow for the barrier to have an increased onshore sediment flux thereby potentially allowing for it to migrate onshore as sea-level rises.

Table 5
Overwash fluxes needed for the barrier to maintain a stable shape and sediment removed from the shoreface based on the minimum and maximum heights of the barrier at each washover and a shoreline retreat rate of −1.4 m/yr.

Pond	Overwash flux necessary (Q_{OW^*})	Sediment removed from shoreface (Q_{SF})
	(m^3/m/yr)	(m^3/m/yr)
Big Homer's Pond: maximum	9.8	20.0
Big Homer's Pond: minimum	7.4	17.6
Long Cove Pond: maximum	12.0	21.1
Long Cove Pond: minimum	7.2	16.3
Edgartown Great Pond: maximum	14.9	21.9
Edgartown Great Pond: minimum	9.3	16.3
Average	10.1	18.9

6. Conclusions

The washovers at Big Homer's and Long Cove Ponds were deposited in 1991 during Hurricane Bob and contain 2.1 and 2.3 × 10^4 m^3 of sediment, respectively. We compute the onshore sediment flux resulting from these overwash events to be about 3.4–2.4 m^3/m/yr. The washover at Edgartown Great Pond was deposited in 1997 during a January nor'easter, contains 2.4 × 10^4 m^3 of sediment, and represents an onshore sediment flux of about 8.5 m^3/m/yr. These values of flux are estimates as they rely on the recurrence intervals obtained from the relatively short tide gauge record and assume that only water levels are necessary to predict when overwash will occur.

The volumes of these washovers are similar to those deposited as confined flows in previous studies (Table 1). The washovers here

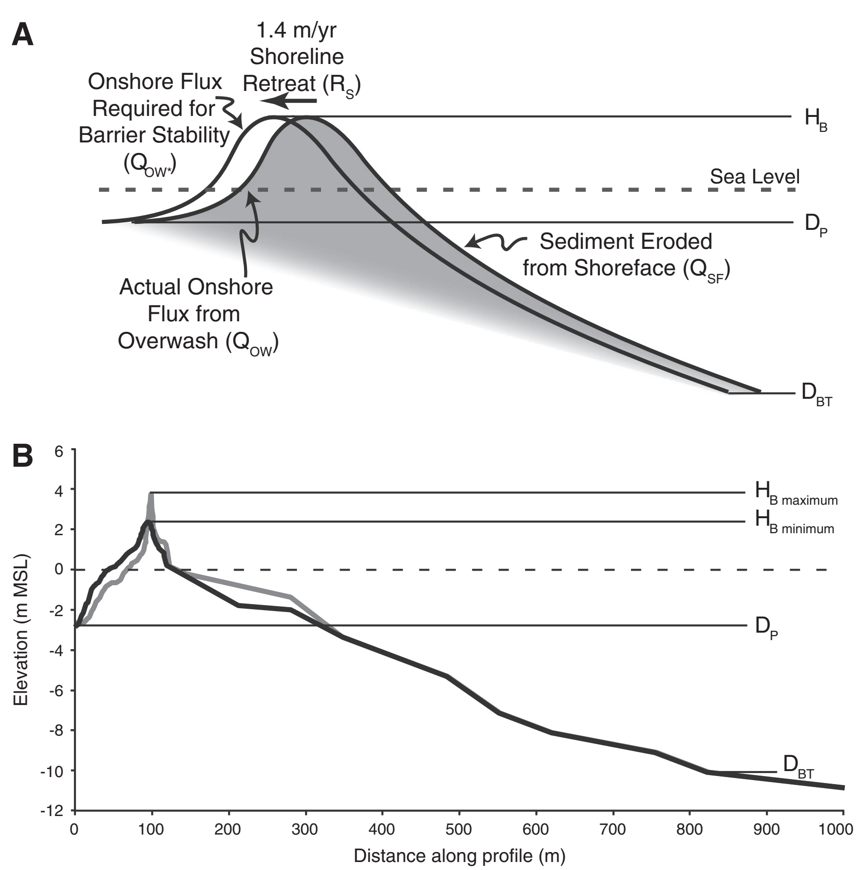

Fig. 9. (A) Schematic depicting the amount of onshore sediment flux, Q_{OW^*}, required to maintain a stable barrier width during shoreline retreat, R_{SF}, related to the actual amount of onshore sediment flux from overwash, Q_{OW}. Heights used in the estimation are the pond depth, D_P, barrier toe depth, D_{BT}, and barrier height, H_B. (B) Heights used in estimation from minimum and maximum from example profiles at Big Homer's Pond.

were confined only by small, erodible dunes that were likely widened during overwash, so the high values may indicate that washover volumes are underestimated when the three dimensional structure of the deposit is not taken into consideration.

The most important conclusion of this study regards barrier evolution. Using a simple geometric model of the barrier retreating at 1.4 m/yr, we estimate an average value of onshore sediment flux needed to maintain the barrier of ~10 m^3/m/yr. This value is higher than the fluxes calculated at Big Homer's and Long Cove Ponds, with the flux at Edgartown Great Pond nearing this value. This result indicates that the barrier is currently out of equilibrium and is thinning under conditions of accelerated sea-level rise and shoreline retreat, a situation confirmed by orthophotos. Assuming continued barrier thinning, more frequent overwash is likely, leading to two possible general outcomes: increased overwash will provide adequate onshore sediment flux to maintain a smaller, thinner barrier, or overwash will remain inadequate, and the barrier will become too small and the barrier will drown. The small barriers of Martha's Vineyard can benefit from sediment supplied by erosion of adjacent headlands. If these barriers were to fail, the inlets or embayments would likely be filled from alongshore sediment sources, a process that has been suggested in the past. Numerical models of barrier evolution are needed to provide insight into which of these options is most likely to occur given estimates of future sea-level rise and storm climate.

Acknowledgements

We would like to thank members of the WHOI Coastal Systems Group for their assistance in the field, lab, and in general, particularly Skye Moret, Stephanie Madsen, Michael Toomey, and Andrea Hawkes. We would also like to thank Christopher Hein for assistance in the field and with editing early drafts of this paper. We would also like to thank Laura Moore and an anonymous reviewer for their thoughtful comments on the manuscript.

D. Philip (Phil) Lane was a valuable member of the Coastal Systems Group as well as a good friend. We dedicate this paper to his memory.

Access to the washovers on South Beach at Long Cove Pond and Big Homer's Pond was graciously provided by the Trustees of Reservations at the Long Pond Reservation. Access to the washover at Edgartown Great Pond was provided by Nancy and Jerry Kohlberg through their caretaker Kendra Buresch. Many thanks to the Martha's Vineyard Coastal Observatory, particularly Janet Fredericks, for allowing the use of the MVCO van on the island. William Wilcox of the Martha's Vineyard Commission proved a valuable resource on the dynamics of the Edgartown Great Pond inlet as well as providing the aerial photos of that washover.

This research was conducted through support from the National Science Foundation, grant #GEO-0815875.

References

Ashton, A.D., Ortiz, A.C., 2011. Overwash control coastal barrier response to sea-level rise. In: Kraus, N.C., Rosati, J.D. (Eds.), Proceedings Coastal Sediments '11. American Society of Civil Engineers Press, New York, pp. 230–243.

Baker, G.S., Jordan, T.E., Pardy, J., 2007. An introduction to ground penetrating radar (GPR). In: Baker, G.S., Jol, H.M. (Eds.), Stratigraphic Analyses Using GPR. Geolologic Society of America Special Puplication, 432, pp. 1–18.

Boothroyd, J.C., Friedrich, N.E., McGinn, S.R., 1985. Geology of microtidal coastal lagoons: Rhode Island. In: Oertel, G.F., Leatherman, S.P. (Eds.), Barrier Islands. Marine Geology, 63, pp. 35–76.

Brown, C.W., 1939. Hurricanes and shoreline changes in Rhode Island. Geographical Review 29, 416–430.

Bruun, P., 1962. Sea-level rise as a cause of shore erosion. Journal of the Waterways and Harbors Division: Proceedings of the American Society of Civil Engineers 88, 117–130.

Buynevich, I.V., FitzGerald, D.M., van Heteren, S., 2004. Sedimentary records of intense storms in Holocene barrier sequences, Maine, USA. Marine Geology 210 (1), 135–148.

Byrnes, M.R., Gingerich, K.J., 1987. Cross-island profile response to Hurricane Gloria. In: Kraus, N.C. (Ed.), Coastal Sediments '87. American Society of Civil Engineers, New York, NY, pp. 1486–1502.

Cheung, K.F., Tang, L., Donnelly, J.P., Scileppi, E.M., Liu, K.-B., Mao, X.-Z., Houston, S.H., Murnane, R.J., 2007. Numerical modeling and field evidence of coastal overwash in southern New England from Hurricane Bob and implications for paleotempestology. Journal of Geophysical Research 112 (F03024).

Cowell, P.J., Roy, P.S., Jones, R.A., 1995. Simulation of large-scale coastal change using a morphological behavior model. Marine Geology 126, 45–61.

Cromwell, J.E., 1971. Barrier coast distribution: a world-wide survey, abstract. Second National Coastal Sallow Water Research Conference, p. 50 (Baton Rouge, LA).

Davis Jr., R.A. (Ed.), 1985. Coastal Sedimentary Environments. Springer-Verlag, New York.

Dean, R.G., Maurmeyer, E.M., 1983. Models for beach profile response. In: Komar, P.D. (Ed.), Handbook of Coastal Processes and Erosion. CRC Press, Boca Raton, Florida, pp. 151–165.

Dillon, W.P., 1970. Submergence effects on a Rhode Island barrier and lagoon inferences on migration of barriers. Journal of Geology 78, 94–106.

Dolan, R., Godfrey, P., 1973. Effects of Hurricane Ginger on the barrier islands of North Carolina. Geological Society of America Bulletin 84, 1329–1334.

Donnelly, J.P., Bryant, S.S., Butler, J., Dowling, J., Fan, L., Hausmann, N., Newby, P.N., Shuman, B., Stern, J., Westover, K., Webb III, T., 2001a. A 700-year sedimentary record of intense hurricane landfalls in southern New England. Geological Society of America Bulletin 113, 714–727.

Donnelly, J.P., Rolls, S., Wengren, M., Butler, J., Lederer, R., Webb III, T., 2001b. Sedimentary evidence of intense-hurricane strikes from New Jersey. Geology 29, 615–618.

Donnelly, C., Kraus, N., Larson, M., 2006. State of knowledge on measurement and modeling of coastal overwash. Journal of Coastal Research 22, 965–991.

Eiser, W.C., Birkemeier, M., 1991. Beach profile response to Hurricane Hugo. In: Kraus, N.C., Gingerich, K.J., Kriebel, D.L. (Eds.), Proceedings Coastal Sediments. Americal Society of Civil Engineers, Seattle, Washington, pp. 1681–1696.

Emanuel, K., Sundararajan, R., Williams, J., 2008. Hurricanes and global warming: results from downscaling IPCC AR4 simulations. Bulletin of the American Meteorological Society 89, 347–367.

Fisher, J.J., Simpson, E.J., 1979. Washover and tidal sedimentation rates as environmental factors in development of a transgressive barrier shoreline. In: Leatherman, S.P. (Ed.), Barrier Islands from the Gulf of St. Lawrence to the Gulf of Mexico. Academic Press, Inc., New York, pp. 127–148.

Fisher, J.S., Stauble, D.K., 1977. Impact of Hurricane Belle on Assateague Island washover. Geology 5, 765–768.

Fisher, J.S., Leatherman, S.P., Perry, F.C., 1974. Overwash processes on Assateague Island. In: O'Brien, M.P. (Ed.), Proceedings of the 14th Conference on Coastal Engineering, Copenhagen, Denmark. American Soceiety of Civil Eengineering, New York, pp. 1194–1211.

FitzGerald, D.M., 1993. Origin and stability of tidal inlets in Massachusetts. In: Aubrey, D.G., Giese, G.S. (Eds.), Formation and Evolution of Multiple Tidal Inlet Systems. American Geophysical Union, Washington, D.C., pp. 1–61.

FitzGerald, D.M., Rosen, P.S., van Heteren, S., 1994. New England barriers. In: Davis, R.A. (Ed.), Geology of Holocene Barrier Island Systems. Springer-Verlag, Berlin, p. 305394.

Frumhoff, P.C., McCarthy, J.J., Melillo, J.M., Moser, S.C., Wuebbles, D.J., 2007. Confronting climate change in the U.S. Northeast: science, impacts, and solutions. Synthesis Report of the Northeast Climate Impacts Assessment (NECIA). Union of Concerned Scientists, Cambridge, MA.

Glaeser, J.D., 1978. Global distribution of barrier islands in terms of tectonic setting. Journal of Geology 86, 283–298.

Hapke, C.J., Himmelstoss, E.A., Kratzmann, M., List, J.H., Thieler, E.R., 2010. National assessment of shoreline change; historical shoreline change along the New England and Mid-Atlantic coasts. U.S. Geological Survey Open-File Report 2010-1118.

Hayes, M.O., 1979. Barrier island morphology as a function of tidal and wave regime. In: Leatherman, S.P. (Ed.), Barrier Islands from the Gulf of St. Lawrence to the Gulf of Mexico. Academic Press, Inc., New York, NY, pp. 1–28.

Howard, A.D., 1939. Hurricane modifications of the offshore bar of Long Island, New York. Geographic Review 29, 400–415.

Inman, D.L., Nordstrom, C.E., 1971. On the tectonic and morphologic classification of coasts. Journal of Geology 79, 1–21.

JALBTCX (Joint Airborne Lidar Bathymetry Technical Center of eXpertise), 2009. 2007 US Army Corps of Engineers (USACE) Topo/Bathy Lidar: Maine, Massachusetts, and Rhode Island.NOAA's Ocean Service (NOS), Coastal Services Center (CSC), Charlotte, SC.

Jelesnianski, C.P., Chen, J., Shaffer, W.A., 1992. SLOSH: Sea, Lake, and Overland Surges from Hurricanes. NOAA Technical Report NWS, 48.

Knapp, K.R., Kruk, M.C., Levinson, D.H., Diamond, H.J., Neumann, C.J., 2010. The International Best Track Archive for Climate Stewardship (IBTrACS): unifying tropical cyclone best track data. Bulletin of American Meteorologic Society 91, 363–376.

Kochel, R.C., Dolan, R., 1986. The role of overwash on a mid-Atlantic coast barrier island. Journal of Geology 94, 902–906.

Landsea, C.W., Anderson, C., Charles, N., Clark, G., Dunion, J., Fernández-Partagás, J., Hungerford, P., Neumann, C., Zimmer, M., 2004. The Atlantic hurricane database reanalysis project: documentation for 1851–1910 alterations and additions to the HURDAT database. In: Liu, K., Murnane, R. (Eds.), Past, Present and Future Hurricanes and Typhoons. Columbia Press, New York, pp. 177–221.

Lane, D.P., 2011. Late Holocene Hurricane Activity and Climate Variability in the Northeastern Gulf of Mexico.Joint Program in Oceanography and Applied Ocean Science and Engineering, Massachusetts Institute of Technology, Department of Earth, Atmospheric, and Planetary Sciences; and the Woods Hole Oceanographic Institution (PhD. Dissertation).

Leatherman, S.P., 1976. Barrier island dynamics: overwash processes and eolian transport. Proceedings of the 15th Conference on Coastal Engineering, Honolulu, Hawaii. American Society of Civil Engineers, New York, pp. 1958–1974.

Leatherman, S.P., 1979a. Beach and dune interactions during storm conditions. The Quarterly Journal of Engineering Geology 12, 281–290.
Leatherman, S.P., 1979b. Migration of Assateague Island, Maryland, by inlet and overwash processes. Geology 7, 104–107.
Leatherman, S.P., 1983. Barrier dynamics and landward migration with Holocene sea-level rise. Nature 301, 415–417.
Leatherman, S.P., 1985. Geomorphic and stratigraphic analysis of Fire Island, New York. In: Oertel, G.F., Leatherman, S.P. (Eds.), Barrier Islands. Marine Geology, 63, pp. 173–195.
Leatherman, S.P., Zaremba, R.E., 1987. Overwash and aeolian processes on a U.S. northeast barrier. Sedimentary Geology 52, 183–206.
Leatherman, S.P., Williams, A.T., Fisher, J.S., 1977. Overwash sedimentation associated with a large-scale northeaster. Marine Geology 24, 109–121.
Lin, N., Emanuel, K.A., Smith, J.A., Vanmarcke, E., 2010. Risk assessment of hurricane storm surge for New York City. Journal of Geophysical Research 115 (D18121).
Liu, K.B., Fearn, M.L., 2000. Reconstruction of prehistoric landfall frequencies of catastrophic hurricanes in northwestern Florida from lake sediment records. Quaternary Research 54, 238–245.
Mayfield, M., 1992. Preliminary Report Hurricane Bob 16–20 August 1991.National Hurricane Center.
Mitrovica, J.X., Gomez, N., Clark, P.U., 2009. The sea-level fingerprinting of West Antarctic collapse. Science 323, 753.
Moore, L.J., List, J.H., Williams, S.J., Stolper, D., 2010. Complexities in barrier island response to sea level rise: insights from numerical model experiments, North Carolina Outer Banks. Journal of Geophysical Research 115 (F03004).
Morton, R.A., Paine, J.G., 1985. Beach and Vegetation-line Changes at Galveston Island, Texas: Erosion, Deposition, and Recovery from Hurricane Alicia.Univ. Texas, Austin, Bureau of Economic Geology Geological Circular, University of Texas, Austin.
Morton, R.A., Sallenger Jr., A.H., 2003. Morphological impacts of extreme storms on sandy beaches and barriers. Journal of Coastal Research 19, 560–573.
Munsell, 2000. Munsell Soil Color Chart.Munsell Color Company, Baltimore, MD.
Nelson, D.D., 1991. Factors effecting beach morphology changes caused by Hurricane Hugo, northern South Carolina. In: Finkl, C.W., Pilkey, O.H. (Eds.), Impacts of Hurricane Hugo, September 10–22, 1989. Journal of Coastal Research Special Issue, 8, pp. 163–179.
Neumann, C.J., Jarvinen, B.R., McAdie, C.J., Elms, J.D., 1993. Tropical cyclones of the North Atlantic Ocean, 1871–1992. National Climatic Data Center National Hurricane Center Historic Climatological Series, 6-2, p. 193.
Nichols, R.L., Marston, A.F., 1939. Shoreline changes in Rhode Island produced by Hurricane of September 21, 1938. Bulletin of the Geological Society of America 50, 1357–1370.
NOAA, 2010. Water level tidal predictions, MA, Martha's Vineyard and Vineyard Sound. http://tidesandcurrents.noaa.gov/tides10/tab2ec1b.html#12 (accessed 1 Dec. 2010).
NOAA, 2011a. Extremes, Newport, RI, Station ID 8452660. http://tidesandcurrents.noaa.gov/data_menu.shtml?extremetype=maxmin&bdate=19300101&edate=20111231&unit=0&format=Apply+Change&stn=8452660+Newport%2C+RI&type=Extremes (accessed 12 May 2011).
NOAA, 2011b. Extremes, Woods Hole, MA, Station ID 8447930. http://tidesandcurrents.noaa.gov/data_menu.shtml?extremetype=maxmin&bdate=19320101&edate=20110608&unit=0&format=Apply+Change&stn=8447930+Woods+Hole%2C+MA&type=Extremes (accessed 12 May 2011).
NOAA, 2011c. Mean sea-level trend 8447930 Woods Hole, MA. http://tidesandcurrents.noaa.gov/sltrends/sltrends_station.shtml?stnid=8447930%20Woods%20Hole,%20MA (accessed 12 May 2011).
Ogden III, J.G., 1974. Shoreline changes along the southeastern coast of Martha's Vineyard, MA for the past 200 years. Quaternary Research 4, 496–508.
Oldale, R.N., 1982. Pleistocene stratigraphy of Nantucket, Martha's Vineyard, the Elizabeth Islands, and Cape Cod, Massachusetts. In: Larson, G.J., Stone, B.D. (Eds.), Late Wisconsinan Glaciation of New England. Kendall/Hunt, Dubuque, IA, pp. 1–34.
Orford, J., Jennings, S., Pethick, J., 2003. Extreme storm effect on gravel dominated barriers. In: Davis, R.A. (Ed.), Proceedings Coastal Sediments'03. World Scientific Press and East Meets West Productions, Corpus Christi, TX.
Pierce, J.W., 1970. Tidal inlets and washover fans. Jouranal of Geolorgy 8, 230–234.
Reardon, L.F., 1926. The Florida Hurricane and Disaster.Miami Publishing Co., Miami, FL.
Redfield, A.C., Miller, A.R., 1957. Water levels accompanying Atlantic coast hurricanes. Meteorological Monitor 2, 1–23.
Sallenger Jr., A.H., 2000. Storm impact scale for barrier islands. Journal of Coastal Research 16, 890–895.
Schwartz, R.K., 1975. Nature and genesis of some storm washover deposits. Coastal Engineering Research Center Technical Memorandum 61.
Simpson, R.H., Hope, J.R., 1971. Atlantic hurricane season of 1971. Monthly Weather Review 100, 256–267.
Stockdon, H.F., Sallenger, A.H., Holman, R.A., Howd, P.A., 2007. A simple model for the large-scale, spatially-variable coastal response to hurricanes. Marine Geology 238, 1–20.
Stolper, D., List, J.H., Thieler, E.R., 2005. Simulating the evolution of coastal morphology and stratigraphy with a new morphological-behaviour model (GEOMBEST). Marine Geology 218, 17–36.
Stutz, M.L., Pilkey, O.H., 2011. Open-ocean barrier islands: global influence of climatic, oceanographic, and depositional settings. Journal of Coastal Research 27, 207–222.
U.S. Army Corps of Engineers, 1963. Operation Five High. North Atlantic Division Report.
Vermeer, M., Rahmstorf, S., 2009. Global sea level linked to global temperature. Proceedings of the National Academy of Sciences 106, 21527–21532.
Viles, H., Spencer, T., 1995. Coastal Problems.Arnold, London.
Wilby, F.B., Young, G.R., Cunningham, C.H., Lieber, A.C., Hale, R.K., Saville, T., O'Brien, M.P., 1939. Inspection of beaches in path of the hurricane of September 21, 1938. Shore and Beach 7, 43–47.
Wolinsky, M.A., Murray, A.B., 2009. A unifying framework for shoreline migration: 2. Application to wave-dominated coasts. Journal of Geophysical Research 114 (F01009).
Woodworth, J.B., Wigglesworth, E., 1934. Geography and geology of the region including Cape Cod, the Elizabeth Islands, Nantucket, Martha's Vineyard, No Mans Land, and Block Island. Harvard College Museum of Comparative Zoology Memoirs 52.